AIAA 2000–0185

Structure of Premixed Turbulent Flames in Flamelet and Thin-Reaction-Zone Regimes

Vaidyanathan Sankaran
and Suresh Menon
School of Aerospace Engineering
Georgia Institute of Technology
Atlanta,GA - 30332

38th AIAA Aerospace Sciences Meeting and Exhibit
January 10–13, 2000 / Reno, NV

Structure of Premixed Turbulent Flames in Flamelet and Thin-Reaction-Zone Regimes

Vaidyanathan Sankaran*
and Suresh Menon†
School of Aerospace Engineering
Georgia Institute of Technology
Atlanta,GA - 30332

The structure of turbulent premixed flame has many facets in practical combustors due to widely varying turbulence-chemistry interactions that can occur. Premixed combustion in the flamelet, the corrugated flamelet and the distributed reaction (recently called the thin-reaction zones) regimes can coexist within the same device. Models used within large-eddy simulation (LES) methodology to simulate practical systems must therefore, be able to predict these space- and time-varying flame structure and propagation characteristics without requiring *ad-hoc* changes. Here, the linear-eddy model (LEM) developed earlier for the flamelet regime has been extended and used to simulate premixed flames over the entire parameter space. A 15-step, 19-species methane-air mechanism has been used in the In-situ Adaptive Tabulation (ISAT) procedure to investigate premixed flame structure from the flamelet,the thin-reaction- zones and well-stirred reactor regimes without any *ad-hoc* modifications. Qualitative and quantitative comparison with experimental observations show that the LEM is capable of capturing the flame structure in flamelet,thin-reaction-zones and well-stirred reactor regimes. This confirms its viability as a practical model for use within LES.

$u^{'}$	=	Rms velocity fluctuation
S_L	=	Laminar flame speed
L	=	Integral length scale
δ_F	=	Flame thickness
T	=	Temperature
Y_k	=	Mass fractions of the kth species
P	=	Thermodynamic pressure
R_u	=	Universal gas constant,
ρ	=	Mass density
$\Delta h^o_{f,k}$	=	Standard heat of formation,at T^o
T^o	=	Standard temperature
$\dot{\omega}_k$	=	Mass reaction rate
$c_{p,k}$	=	Specific heat at constant pressure
W_k	=	Molecular weight of kth species
$\bar{c}_p$	=	Mixture averaged specific heat at constant pressure
$\bar{\kappa}$	=	Mixture averaged thermal conductivity
D_k	=	Mixture averaged mass diffusivity of the 'kth' species
C	=	Progress variable $1 - Y_{CH_4}/Y^o{}_{CH_4}$
$Y^o{}_{CH_4}$	=	Initial CH_4 mass fraction
Re	=	$u^{'}L/\nu$
Da	=	$(L/\delta_F)\ /\ (u^{'}/S_L)$
Ka	=	$(\delta_F/\eta)^2$
η	=	$N_\eta * L * Re^{-3/4}$

*Graduate Research Assistant,Student Member
†Professor, AIAA Senior Member

1 Introduction

Study of premixed turbulent flames has occupied a primary area in combustion research since the days of Damkohler due to the wealth of knowledge it provides about turbulent reacting flows. Understanding the structure of premixed turbulent flames can help in the design of safer, more efficient and environment friendly combustion devices such as internal combustion engines, ramjets and industrial furnaces. But due to the wide spectrum of length and time scales present in real combustion systems, more than one mode of combustion often co-exists. The characteristics such as the propagation speed and flame structure can be different depending upon the local values of the velocity ratio u'/S_L and the length scale ratio L/δ_F.

Combustion diagrams such as the one shown in Fig. 1 have been used to characterize the structure of the premixed flame, similar to the phase diagrams proposed by Borghi,[1] Peters,[2] Bray[3] and Williams.[4]

In such a diagram, in addition to u'/S_L and L/δ_F, various non-dimensional numbers such as Damkohler number Da, Karlovitz number Ka and Reynold's number Re, are used to demarcate different regimes. Depending on the dynamics determined by these non-dimensional numbers, flame structure can be drastically different.

For instance in the limit of large Damkohler number (Da >>1), and low Karlovitz number (Ka < 1), turbulent flame brush can be considered as an ensemble of laminar flames wrinkled by turbulent eddies. In this regime, chemical time scales are much smaller than

the turbulent time scales. Combustion takes place in a thin continuous flame sheet propagating locally at the laminar flame speed in a direction normal to itself. Since the chemistry and turbulence are decoupled, turbulence only wrinkles and corrugates the flame sheet. This is called the flamelet regime.

In the limit of low Damkohler number (Da $<$ 1) and high Karlovitz number (Ka $>$ 1), time scales of the turbulence are of the same order or even smaller than that of chemical reactions. Therefore, high intensity eddies can interact with the flame thus, altering or even inhibiting its propagation (resulting in flame quenching). This regime is known as the well-stirred reactor regime.

In-between these two extremes lies the distributed reaction regime, where Karlovitz number is greater than unity (Ka $>$ 1). In this regime turbulent scales are of the order of chemical scales and a strong flame/turbulence interaction is present here. Flame sheets are no longer continuous due to local quenching. The transition from flamelet to the distributed reaction regime is marked by a line corresponding to unity Karlovitz number, and is referred to as the Klimov-Williams (K-W) limit. As the K-W limit is crossed turbulent eddies may enter the reaction zone, causing the flame to quench due to excessive stretch. But recently, Peters[5] has proposed that the flamelet-like structures would exist even beyond the K-W limit. The argument is that the smallest eddies can only enter the preheat zone thus, increasing turbulent transport of heat and species away from it. Scales of the order of Kolmogorov eddies are dissipated even before they reach the reaction zone, because of the increased viscosity near the flame. Thus the flames in this regime have thick preheat zone followed by thin reaction zones. So this regime is called the thin-reaction-zone regime.

Combustion models which attempt to predict various performance parameters like local heat release, NO_X and CO emissions and combustion efficiency, must be able to capture the characteristics of the combustion in all the regimes without any ad-hoc fixes. Unfortunately combustion models developed in the past have focussed only on particular regimes. For instance, the G- equation model,[6] solves a model equation for the propagation of a thin flame by convective transport and is restricted to the flamelet regime. Similarly PDF models,[7] require different diffusion models for different regimes.

The objective of this work is to demonstrate a model that can be applied in the entire parameter space of premixed combustion without requiring any *ad hoc* adjustments. In this study, the linear eddy mixing (LEM) model of Kerstein,[8] which was previously demonstrated in the flamelet regime,[9–11] has been used to study premixed combustion in the flamelet thin-reaction-zone and well-stirred reactor regimes

LEM is a stochastic model of turbulence kinematics implemented as a Monte Carlo simulation to compute statistical properties of the scalar fields in stationary and decaying homogeneous turbulence in free and wall bounded shear flows. LEM treats the two different mechanisms, molecular diffusion and turbulent convection, that govern the evolution of a scalar separately and concurrently.

In this study we simulated the methane-air flames B1, F1 and F3 that were recently studied by Chen *et al*[12] and Mansour *et al*.[13] The typical location of these flames are given in Fig. 1. As shown, B1 is in the corrugated flamelet regime, F3 is in the thin-reaction-zone regime, close to the border of the flamelet regime while F1 is deep in the distributed reaction zone. In order to study the flame structure in the well stirred reactor regime, where local flame extinction can occur, a flame F0 which is near the lean-extinction limit is also simulated.

2 Model Formulation

LEM is a stochastic model which treats the two mechanisms viz., diffusion and turbulent convection separately but concurrently. Molecular diffusion is handled by numerical integration of the one dimensional scalar diffusion equation. Within this one dimensional domain, the equations governing constant pressure,adiabatic laminar flame propagation are

$$\frac{\partial Y_k}{\partial t} = -\frac{1}{\rho}\frac{\partial \rho Y_k V_k}{\partial x} + \frac{\dot{\omega}_k W_k}{\rho} + F_{k\,stir} \qquad (1)$$

$$\begin{aligned}\frac{\partial T}{\partial t} &= -\frac{1}{\rho}c_p \sum_{k=1}^{N} c_{p,k} Y_k V_k \frac{\partial T}{\partial x} + \\ &\frac{1}{\rho \bar{c}_p}\frac{\partial}{\partial x}(\bar{\kappa}\frac{\partial T}{\partial x}) - \\ &\frac{1}{\rho \bar{c}_p}\sum_{k=1}^{N} h_k \dot{\omega}_k W_k + F_{T\,stir}\end{aligned} \qquad (2)$$

and the equation of state

$$P = \rho T \sum_{k=1}^{N} Y_k R_u / W_k \qquad (3)$$

$$h_k = \Delta h^{\circ}_{f,k} + \int_{T^{\circ}}^{T} c_{p,k}(T')dT' \qquad (4)$$

Here V_k is the diffusion velocity of the 'kth' species. The mixture averaged specific heat at constant pressure and thermal conductivity are, $\bar{c}_p$ and $\bar{\kappa}$, respectively. Diffusion velocity is defined as

$$V_k = -\frac{D_k}{Y_k}\frac{dY_k}{dx} \qquad (5)$$

where D_k is the mixture averaged diffusivity of the 'kth' species.

Since turbulent convection is implemented explicitly, the convective terms $u\partial Y_k/\partial x$ and $u\partial T/\partial x$ in the species and energy equations are symbolically represented as $F_{k\,stir}$ and $F_{T\,stir}$, respectively. These terms are implemented using stochastic rearrangement events called triplet maps, each of which represents the action of a turbulent eddy on the scalar fields.

LEM relates fluid element diffusivity to the random walk of a marker particle. The total turbulent diffusion of a marker particle caused by eddies of size ranging from L to η, based on the triplet mapping[8] is given by

$$D_T \approx \nu(L/\eta)^{4/3} = \frac{2}{27}\lambda \int_\eta^L l^3 f(l) dl \qquad (6)$$

Turbulent convection is implemented as a random rearrangement of the scalar field along the linear eddy domain. This rearrangement mimics the action of individual eddies on the scalar field. Three quantities govern each stirring event: the eddy size, location and the rate of stirring. The size is determined randomly from a PDF of eddy sizes given by

$$f(l) = \frac{5}{3}\frac{l^{-8/3}}{\eta^{-5/3} - L^{-5/3}} \qquad (7)$$

in the range $\eta < l < L$ (obtained from inertial range scaling[8]) The event location is randomly chosen from a uniform distribution within the one-dimensional domain. The eddy sizes and event rate (frequency per unit length) are determined from (6) and an equivalent expression for the turbulent diffusivity,[8] $D_T = u' L/C_\lambda$, where C_λ is a model constant.

The event rate is determined as $E = \lambda X_{LEM}$, where X_{LEM} is the length of the one-dimensional domain and λ is the event frequency per unit length which is determined by[8]

$$\lambda = \frac{54}{5}\frac{\nu Re}{C_\lambda L^3}\frac{[(L/\eta)^{5/3} - 1]}{[1 - (\eta/L)^{4/3}]} \qquad (8)$$

The time interval between events is then given as $\Delta t_{stir} = 1/(\lambda X_{LEM})$ Here, η is determined from the familiar inertial range scaling law $\eta = N_\eta L Re^{-3/4}$ where N_η is an empirical constant.

In order to predict the turbulent flame speed and to compare with experimental data, it is necessary to determine the two calibration constants. The first constant C_λ is introduced to scale the experimental turbulent diffusivity with the model turbulent diffusivity. The second constant N_η is an empirical constant to scale the Kolmogorov scale η. This reduces the effective range of scale between L and η, but does not change the turbulent diffusivity since the probability of eddy distribution is normalized to unity. In the earlier studies,[11] these parameters were obtained by comparing LEM predictions to experimental data[14] in the flamelet regime. The present study uses these same values in order to determine if the LEM model validated in the flamelet regime can be applied to flames in the thin-reaction-zones regime without any adjustments.

Once the event size and location are determined using the above mentioned expressions, the rearrangement event is implemented using the triplet mapping. Details of the triplet mapping and its implementation are given elsewhere.[11] Numerical setup and the methodology adapted to handle finite rate effects are discussed in the following section.

3 Numerical Implementation

Methane-air flames similar to those in the experiments are studied here. In order to obtain a realistic chemical state over a wide range of operating conditions, a 15-step, 19-reaction skeletal mechanism[15] is employed and is given in Table 5. This mechanism (which included NOx kinetics) has been shown to be quite accurate over a wide range of equivalence ratios. It is also capable of predicting extinction and re-ignition which is particularly relevant here since the F0 flame is in the well stirred reactor zone where partial local quenching can occur.

The numerical method is the same as in the earlier study[10,11] and therefore, only briefly summarized. To simulate a stationary flame, a moving observation window is used that translates with the flame brush to maintain approximately the same relative position between flame center and observation window (even though the flame propagates freely into the reactants). All statistics are obtained relative to the flame center. Further details are given elsewhere.[10,11] The computational domain is chosen large enough to fully capture this flame brush (typically $6L$). Earlier studies[10,11] and the present study show that statistically, stationary flames can be simulated using this approach.

A backward Euler time integration scheme is employed for the time integration of the reaction-diffusion equations (1) and (2). All spatial derivatives were discretized using a second-order accurate central difference schemes. A fractional step method known as zeroth-order operator splitting[16] is used to handle the chemistry. In this type of splitting, the evolution equations for pure mixing system (omitting reaction terms) is integrated for a small time step δt to get the ϕ_{mix}, which represents the thermo-chemical state after mixing. Then, the pure reaction system is integrated from initial conditions ϕ_{mix} over a time step δt to get $\phi(t + \delta t)$.

A linear stability analysis of the backward Euler time integration, limits the maximum diffusion time step to $\Delta t_{diff} = C_{diff}\Delta X_{LEM}^2/D_{max}$, with $C_{diff} = 0.5$. Here, ΔX_{LEM} is the cell size used to discretize the LEM domain. A value of $C_{diff} = 0.25$ is used for the explicit integration to give some margin of safety.

Maximum diffusion coefficient is calculated from the pre-specified lewis numbers. These lewis numbers are constant but different for each species and are calculated using CHEMKIN at the product temperature. Dufort, Soret and pressure diffusion effects have been neglected in the present study.

3.1 *In situ* Adaptive Tabulation

As a result of the operator splitting employed for the source terms in the scalar equation, the temporal evolution of species and energy due to chemical reaction is governed by a system of ordinary differential equations, of the form

$$\frac{d\phi}{dt} = \dot{\omega}(Y_k, T, P) \tag{9}$$

These equations constitute a stiff system with a wide spectrum of characteristic evolution time scales. Integration of (9) requires specialized solvers[17] which are in general computationally expensive. Hence, Direct Integration (DI) is normally impractical. Therefore, most of the approaches[18] resort to pre-calculation and tabulation of the thermochemistry. These tables store information about the thermo-chemical variables at the end of a given time step as a function of the initial state of the thermo-chemical variables. But this does not seem to alleviate the problem, since accessibility to the stored information requires complex interpolation, not to mention the errors introduced by the interpolation. Also storage requirements grow with the dimension of the problem (which is dictated by the number of species involved). A new technique called In-situ Adaptive Tabulation[19] (ISAT) is used in this work to efficiently handle finite-rate kinetics.

In ISAT, only the accessed region of the composition space is tabulated instead of the whole realizable region. Accessible region is defined as the phase space (or composition space) of all composition that occurs in a reacting flow computation. Realizable region is the set of all possible combinations of compositions for a given number of species. Since the accessible region of composition space depends on many aspects of the flow such as transport processes and kinetics, it is only a subset of the realizable space. Since ISAT builds a table only for the accessible region, overall time required to build, retrieve and store information reduces significantly. Also, this tabulation is done as the flow computation proceeds instead of constructing *apriori*. Therfore, each entry in the table corresponds to a composition that occurs in the reactive flow calculation.

3.2 ISAT Algorithm

Reactive flow calculation provides the ISAT code with the time step δt (i.e., usually of the order of the diffusion scale) and a set of initial chemical state to be updated. An acceptable error tolerance for each of the species mass fractions to control the local tabulation error is also provided to the ISAT code. The initial chemical state is called the query composition. Given the query, if it is the very first query a first record called leaf is generated by integrating the governing equation (9). This initializes the binary tree to a single leaf. For the subsequent queries the tree/table is traversed until a record is reached. A record or leaf in a table consists of initial composition, ϕ^o, sensitivity matrix $S(\phi^o)$, integrated solution $R(\phi^o)$ of the initial composition ϕ^o and the specification of an ellipsoid of accuracy (EOA).[19] Ellipsoid of accuracy is an ellipsoidal region, centered at ϕ^o, within which the linear approximation given by

$$R^l(\phi^q) \approx R(\phi^o) + S(\phi^o)(\phi^q - \phi^o) \tag{10}$$

is known to be accurate. $R^l(\phi^q)$ is the linear approximation of the solution to the query composition ϕ^q. Once a record/leaf close (in some sense) to the query composition is reached, the difference between the query and the leaf is estimated. If this is within the EOA then the linear approximation (10) is used to return the result. This process is called a retrieve. If the query is outside the EOA, then a direct integration is performed to determine the chemical state after reaction and the error ϵ is determined, where

$$\epsilon = R(\phi^q) - R^l(\phi^q) \tag{11}$$

and $R(\phi^q)$ is the result of direct integration of the equation (numerically exact solution) to the query composition. If the error is within the acceptable tolerance ($\epsilon < \epsilon_{tol}$), it signifies that the region over which the linear approximation (10) is accurate (EOA) is bigger than the current EOA. So the EOA is grown. This process is called growth. If ($\epsilon > \epsilon_{tol}$) then a new leaf is generated based on the numerical integration from the query composition. As the computation proceeds, with increasing probability, query composition lies within the EOA of the table entry ϕ^o. After sufficiently long time, ISAT will be retrieving the result from the table most of the time rather than integrating the stiff equations all the time.

3.3 ISAT Efficiency

Efficiency of ISAT in handling the finite rate kinetics for detailed chemistry is reported here. ISAT performance in LEM simulations is measured by observing the time spent on chemistry by direct integration (DI) and ISAT approach. Speed-up is defined as follows.

$$\text{Speed-up} = \frac{\text{CPU time for N steps with DI}}{\text{CPU time for N steps with ISAT}}$$

N should be sufficiently large for the ISAT algorithm to be effective. The local error defined as the difference between the result obtained by direct integration and by using ISAT for a given initial chemical state is controlled by specifying the tolerance parameter ϵ_{tol}. This

determines the allowable error in each of the scalar for a given initial state. This parameter also determines the number of records that will be present in the table. For higher accuracy, this parameter should be low leading to an increase in the total simulation time and storage. A ϵ_{tol} of 0.0008 was used in this simulation. Table 4 compares the performance of ISAT against the direct integration. A speed-up of 31 is achieved by ISAT approach, which almost reduces the total simulation time to one-third.

3.4 Parallel Implementation

Stand-alone LEM simulations with ISAT-chemistry was implemented on multi-processor, distributed memory parallel processing computer using Message Passing Interface (MPI).

By employing an operator splitting for the source terms, the set of governing equations (1)-(4) can be split into two sets of equations. One set of equations governing the evolution of species and temperature under diffusion and another set of equations (9) governing the temporal evolution of scalars due to chemical reactions. Convective terms are handled separately by LEM stirring. A type of parallelism known as data parallelism, is used here. In this approach, the computational domain is divided into smaller sub-domains which are assigned to different processors. Mapping of processors to the computational grid is done in terms of grid numbers instead of the physical co-ordinates. Each processor has an identical copy of the numerical algorithm and works on a small region simultaneously, exchanging appropriate data with its neighbor at the processor boundaries.

The chemistry solver is a point problem, so no communication is needed to solve equations (9). Each processor uses the ISAT algorithm to build a table for the set of composition that occurs only inside its domain, during the computation. This way of localizing the chemistry and table to each processor reduces the overall load for each processor, as opposed to building a single table for all the composition that occurs over the whole of the domain. Also this reduces the searching time involved in the process of retrieving data from the table. Simulations were done on a 32 processor CRAY-T3E systems.

4 Results And Discussion

Results obtained using the LEM simulations for freely propagating turbulent flames are presented here. Comparison of predicted turbulent flame speed and flame structure are made against the high Reynolds number fan stirred bomb experiments of Abdel-Gayed *et al*[14] and highly stretched turbulent premixed flames.[12,13]

4.1 Instantaneous Flame Structure

The LEM simulations were carried out long enough to obtain sufficient data for statistical analysis. Instantaneous images of the flame structure were also obtained and typical images of the temperature and the destruction rate of methane, $\dot{\omega}_{CH_4}$ for the B1, F3 and F1 flames are shown in Figure 2. Tables 1 and 2 summarize the properties of these flames. We use $\dot{\omega}_{CH_4}$ to identify the location of the reaction zone (CH is not available in the skeletal mechanism) since it has been shown to correlate well with the location of the reaction zone.[20] The transition from the flamelet (Flame B1) to the structure seen in the thin-reaction-zones regime (Flames F3 and F1) is clearly apparent in these figures. For Flame B1, the preheat zone upstream of the flame zone is inert with its temperature close to the free stream value. However, as Ka and Re increases, eddies penetrate into the preheat zone and increase the temperature ahead of the flame brush. As one progresses from Flame B1 to F3 and to F1, the temperature increase in the preheat zone increases. However, the reaction zone still remains localized and thin in all cases with $\dot{\omega}_{CH_4}$ peaking at location of steep temperature gradients. Even though at unity Karlovitz number, $\eta \approx \delta_F$, the smallest eddies are not still small enough to enter the inner layer, where, in an asymptotical sense the main reaction zone might be assumed. Typically, inner layer is one-tenth of the flame thickness,[21] which is much smaller than η. Thus, small eddies can only enter the preheat zone, while the inner layer is practically unaffected. This is well portrayed by the reaction rate profiles. A very good qualitative agreement of the temperature profiles with the experimental data (Figure 2d from Mansour *et al*[13]) was also observed. The reaction zone thickness is estimated to be 0.16 mm and 0.27 mm for F1 and F3 flames, respectively. These values are very close to the laminar flame thickness of 0.175 mm.[12] Experimental data[13] for CH suggests a value in the range 0.2-0.5 mm for the F3 and F1 flames.

Although the reaction zone is thin and of the order of the laminar flame thickness, the preheat zone is much larger. Using the definition[13] that the preheat zone is between temperature 600 K and 1300 K, the thickness of the preheat zone δ_{PHZ} is estimated as 2.2 mm and 1.92 mm for the flames F1 and F3, respectively. In the recent experiments[13] the preheat zone thickness was estimated in the range 2-3.5 mm for Flame F1 (no other data is currently available). Presence of such thin reaction zones, with thick preheat zone in front, is characteristic of flames in thin-reaction-zone regime. Note that $\eta = 0.05$ mm and 0.1 mm for the F1 and F3 flames, respectively.[12] Thus, the preheat zone thickness is much larger than η.

4.2 Flame Structure in Well-Stirred Reactor Regime

A flame in the well-stirred reactor regime was also investigated. The non dimensional parameters are chosen so that flames will be subject to local extinc-

tion.

Instantaneous profiles of the temperature at three arbitrarily chosen times are shown in Figure 3. Three distinct flame structures can be observed from the temperature profiles. In Figure 3a the flame seems to exhibit a behavior similar to the flames in thin-reaction-zone regime, with a thick preheat zone and a localized thin-reaction-zone. Destruction rate of methane, $\dot{\omega}_{CH_4}$ shows the presence of a thin reaction zone and a thick inert preheat zone ahead of it.

Figure 3b shows the structure of the flame at an instant when the flame has been quenched partially/locally (in time). Significantly weakened concentrations of OH species was observed at this instant. Detailed vortex-flame interaction experiments[22] at very lean methane-air mixtures also indicate that OH concentration decreases considerably during quenching. Reaction rate profile also shows that not much of reaction occur in the flame indicating that strong eddies have perturbed the the inner layer. An estimate of the reaction zone thickness showed that the inner layer thickness is of the order of the Kolmogorov scale, when partial quenching occurred. Thus the modification of inner layer must be the reason for flame quenching rather than the modification of the preheat zone.

In Figure 3c it can be observed that in some parts of the flame even though the temperature is around 1500 K, no significant reaction seems to be going on. Reaction rate profiles of methane and the instantaneous profiles of OH species (Figure 3d) provide evidence for the little reaction that goes on in this region indicating the presence of hot non-reacted holes. This indicates that an eddy with the extinction strain rate must have perturbed the inner layer.

These observations about the flames in the well-stirred reactor regime are also consistent with the observations of Dinkelacker *et al*,[23] who conducted experiments at similar conditions.

4.3 Mean Flame Structure

The transition from flamelet to thin-reaction-zones regime combustion is best presented by the probability density function (PDF) of C. Figure 4. shows the PDF of the progress variable at six different locations for the flames B1, F3, F1 and F0.

It is clear that when combustion occurs in flamelets, the probability density function of the progress variable must exhibit two peaks, one corresponding to un burnt gases and the other corresponding to burnt products.[24] Bimodal PDF of B1 flames clearly show that it is in the flamelet regime, where the interaction between turbulence and combustion is purely kinematic (does not depend on th length scales). In this regime probability of the reactive states corresponding to the transition between reactants and products is small. This is because the probability of a measuring probe (or a sample point in numerical experiment) to be in burnt side or un burnt side would be higher. The probability of the probe to be inside the flame where most of the reaction goes on is very low since the flame thickness is so small in the laminar flamelet regime.

Figure 4b, 4c and 4d shows respectively, the PDF of the progress variable of the flames F3, F1 and F0. Distributed nature of the PDF clearly shows that the probabilities of intermediate values of C, increases as we move more and more into the thin reaction zone and well-stirred reactor reaction regimes. Small eddies that enter the preheat zone broaden the flame increasing the probability of intermediate values of progress variable. This is in excellent qualitative agreement with the progress variable PDF's reported in[24] for flames in similar regimes.

The mean temperature profiles for all the flames are shown in Figure 5 as a function of X/L (note that L is much larger for B1, see Table 1). A direct comparison shows that as Ka increases the flame brush thickness increases, which results in a broadened mean temperature profile. An increase in preheat zone thickness can be observed as we move from flamelet to distributed regime. The thickness of the preheat zone is of the order of the integral length for all the F-flames. This suggests that eddy as large as L are involved in the transport of heat and mass from the reaction zone into the preheat zone.

Mean and variance of the progress variable, C have also been computed. Progress variable seems to exhibit a behavior similar to the mean temperature profile across the flame. A measure of the scalar dissipation is obtained from the scalar variance profiles since regions of high scalar variances indicate low scalar dissipation rate and vice versa. Variance of the progress variable for F1, F2 and F3 are shown in Figure 6. Results show that F1 has a lower maximum scalar variance when compared to F3. This indicates that F1 flames have higher scalar dissipation rate. Presence of more small scale wrinkling in the inner layer of F1 could be the reason for the increased scalar dissipation in F1.

4.4 Mean Species Structure

Figure 7 and Figure 8 shows, respectively the mean profiles of the major species, CH_4, O_2 and CO_2 and the profiles of the minor species OH, NO and CO across flame-brush. Each mean profile is an average of over 700 instantaneous profiles. Decrease of reactant mass fraction and increase of product mass fraction across the flame is consistent with the premixed flame theory. Mass fraction profiles of CO reveal the approximate location of reaction zone. It peaks near the rection zone and falls off in the post flame zone, where it is oxidized to CO_2 by OH. Mean OH profile also shows a similar trend.

Mean NO mass profile for the four flames are presented in Figure 9. It can be observed that the NO

mass fraction increases with the increase in temperature. This is due to the formation of NO by thermal NO mechanism. NO mass fraction is at its least for the F0 flames and highest for the F3 flame. This is because F0 corresponds to flames in well-stirred reactor regime, where mixing due to small scale turbulence is very effective in producing an almost homogeneous mixture. Also F0 flames corresponds to a lean mixture of equivalence ratio 0.6, whereas F3 corresponds to the stoichiometric mixture in the thin-reaction-zone regime. Thus, lean premixed atmospheric combustion seems to reduce the pollutant formation. Although F1 and F3 have the same equivalence ratio, F1 seems to produce less NO compared to F3. Reason could be attributed to the fact that F1 is closer to the well-stirred reactor regime than F3.

4.5 Turbulent Propagation Speed

Turbulent propagation speed is determined from the time trace of the propagation of the leading flame.[25] Time traces of the four CH4-Air flames simulated using LEM are shown in Figure 10. All of them exhibits an almost constant propagation speed after a short initial transition. Propagation speed is determined from the slope of the time traces. Simulated results of B1 flames corresponds to the fan-stirred bomb experiments.[14] An u_t/S_L of 4.7 was reported for the B1 flame with $u^{'}/S_L$ of 1.733. LEM predicts under similar conditions a u_t/S_L of 4.81. LEM's over-prediction of the flame speed could be due to the variation in the model turbulent diffusivity. In an attempt to compare LEM results with other model predictions, an estimate of turbulent flame speed is made with the u_t/S_L expression given by Peters[5] for similar conditions using G-equation model. LEM prediction closely follows the trend in variation of u_t/S_L for varying $u^{'}/S_L$ and L/δ_F. Values of u_t/S_L for the various flames are given in Table 3. In the thin-reaction-zones and well-stirred reactor regime small eddies that enter into the preheat zone will destroy the quasi-steady flame structure that exists in the corrugated flamelet regime. Therefore, a steady-state burning velocity cannot be defined anymore. So the value of u_t/S_L reported here does not have any physical meaning.

5 Conclusion

Structure of the premixed freely propagating turbulent flames in various combustion regimes have been investigated using a scalar mixing model. The flames simulated closely corresponded to flames studied in recent experiments and range from the flamelet regime to the well-stirred reactor regime. The LEM model validated earlier for the flamelet regime was used without any modification to study all these flames. A skeletal methane-air mechanism was used within an ISAT algorithm to significantly reduce the computational effort. Results show reasonable agreement with past experimental observations and confirm the flamelet nature of the thin-reaction-zones regime. Also, the structure of the flames predicted by LEM in the well-stirred reactor regime matches the recent experimental observations in these regimes.

The LEM model appears capable of capturing quantitatively the structure and propagation characteristics of turbulent premixed flames over a wide range of operational parameters without requiring any adjustments. The computational efficiency gained by using the ISAT procedure also provides the confidence that the LEM model with skeletal kinetics is a good candidate for a sub-grid combustion model for LES applications. This is particularly important since turbulence and combustion conditions can vary widely within the same device and the simulation model must be capable of dealing with these regimes without requiring *ad hoc* fixes. The past use of LEM for sub-grid non-premixed[26] and premixed flamelet combustion[11,27] and the present study confirms that LEM is a viable sub-grid combustion model regardless of the nature of combustion. Application of LEM within LES using the ISAT procedure is currently underway and will be reported in the near future.

References

[1] Borghi, R., *Recent Advances in Aerospace Sciences*, Plenum,N.Y., 1985.

[2] Peters, N., "Laminar Flamelet Concepts in Turbulent Combustion," *Twenty-First Symposium (International) on Combustion*, 1986, pp. 1231–1250.

[3] Bray, K., Libby, P., and Williams, F., *Turbulent Reacting Flows*, Springer-Verlag, 1980.

[4] Williams, F., *Mathematics of Combustion*, SIAM, Philadelphia, 1985.

[5] Peters, N., "The turbulent Burning Velocity for Large-scale and small scale turbulence," *Journal of Fluid mechanics*, Vol. 384, 1999, pp. 107–132.

[6] Kerstein, A., Wm.T., A., and William, F., "The Field Equation for Interface Propagation in an Unsteady Homogenous Flow Field," *Phys. Rev. A*,, Vol. 37, 1988, pp. 2728.

[7] Pope, S. and Anand, M., "Flamelet and Distributed Combustion in Premixed Turbulent Flames," *Twentieth Symposium (International) on Combustion*, 1984, pp. 403–410.

[8] Kerstein, A. R., "Linear-Eddy Modeling of Turbulent Transport. Part 6. Microstructure of Diffusive Scalar Mixing Fields," *Journal of Fluid Mechanics*, Vol. 231, 1991, pp. 361–394.

[9] Menon, S., McMurtry, P., and Kerstein, A. R., "A Linear Eddy Mixing Model for Large Eddy Simulation of Turbulent Combustion," *LES of Complex Engineering and Geophysical Flows*, edited by B. Galperin and S. Orszag, Cambridge University Press, 1993.

[10] Smith, T. M. and Menon, S., "Model Simulations of Freely Propagating Turbulent Premixed Flames," *Twenty-sixth Symposium (International) on Combustion*, 1996, pp. 299–306.

[11] Smith, T. M. and Menon, S., "One-Dimensional Simulations of Freely Propagating Turbulent Premixed Flames," *Combustion Science and Technology*, Vol. 128, 1996, pp. 99–130.

[12] Chen.Y.C., Peters, N., Schneemann.G.A.i, Wruck.N.i, Renz.U., and ansour.M.S., "The Detailed Structure of Highly Stretched Turbulent Premixed Methane-Air Flames," *Combustion and Flame*, Vol. 107, 1996, pp. 223–244.

[13] Mansour, M., Peters, N., and Chen, Y., "Investigation of Scalar Mixing in the Thin Reaction Zones Regime using a simultaneous CH-LIF/Rayleigh Laser Technique," *Twenty-Seventh Symposium (International) on Combustion*, 1998, pp. 767–773.

[14] Abdel-Gayed.R.G., Al-Khishali.K.J., and Bradley.D., "Turbulent Burning Velocities and Flame Straining in Explosions," *Proceedings of the Royal Society of London A*, Vol. 39, 1984, pp. 393.

[15] Chen.Y.J., "Private Communication," 1999.

[16] Calhoon, W., Menon, S., and Goldin, G., "Comparison of Reduced and Full Chemical Mechanisms for Nonpremixed Turbulent H2-Air Jet Flames," *Combustion Science and Technology*, Vol. 104, 1995, pp. 115.

[17] Hindmarsh.A.C., Stepleman.R.S. etal, E., *Scientific Computing*, North-Holland, Amsterland, 1983.

[18] Chen, J., Chang, W., and Koszykowski.M, "Numerical Simulation and Scaling of NOx Emissions from Turbulent Hydrogen Jet Flames with Various Amounts of Helium Dilution," *Combustion Science and Technology*, Vol. 110, 1995, pp. 505–529.

[19] Pope, S., "Computationally Efficient implementation of combustion chemistry using in situ adaptive tabulation," *Combustion Theory Modelling*, Vol. 1, 1997, pp. 41–63.

[20] Najm, H. N., Paul, P. H., Mueller, C. J., and Wyckoff, P. S., "On the Adequacy of Certain Experimental Observables as Measurements of Flame Burning Rate," *Combustion and Flame*, Vol. 113, 1998, pp. 312–332.

[21] Seshadri, K. and Peters.N., *Combustion and Flame*, Vol. 81, 1990, pp. 96–118.

[22] Poinsot, T., Veynante, D., and Candel, S., *Journal of Fluid mechanics*, Vol. 228, 1991, pp. 561–606.

[23] Dinkelacker.F., Soika.A., Most.D., Hofmann.D., Leipertz.A., Polifke.W., and Dobbeling.K., *Twenty-seventh Symposium (International) on Combustion*, 1999, pp. 857–865.

[24] Duarte.D., Ferrao.P., and Heitor.M.V., "Turbulence Statistics and Scalar Transport in Highly Sheared Premixed flames," *Flow,Turbulence and Combustion*, Vol. 60, 1999, pp. 361–376.

[25] Kerstein, A. R., "Pair-Exchange Model of Turbulent Premixed Flame Propagation," *Twenty-First Symposium (International) on Combustion*, 1986, pp. 1281–1289.

[26] Menon, S. and Calhoon, W., "Subgrid Mixing and Molecular Transport Modeling for Large-Eddy Simulations of Turbulent Reacting Flows," *Twenty-Sixth Symposium (International) on Combustion*, 1996, pp. 59–66.

[27] Chakravarthy, V. K. and Menon, S., "Modeling of turbulent premixed flames in the flamet regime," *First Symposium on Turbulence and Shear Flow Phenomena*, 1999.

Table 1 Turbulent Flame Properties

Flame	ϕ	S_L m/sec	δ_F mm	u' m/sec	L mm
B1	0.8	0.30	0.233	0.52	15.0
F3	1.0	0.40	0.175	4.76	2.4
F1	1.0	0.40	0.175	2.12	2.4
F0	0.6	0.11	0.636	3.70	10.0

Table 2 Non-Dimensional quantities

Flame	u'/S_L	L/δ_F	Re	Da	Ka
B1	1.733	64.28	496	37.08	0.817
F3	5.313	13.71	73	2.580	23.00
F1	11.90	13.71	164	1.152	91.00
F0	33.64	15.72	529	0.465	421.0

Table 3 Turbulent Flame Properties

Flame	u_t/S_L Expt.	u_t/S_L LEM	u_t/S_L Peters'	δ_{PHZ} mm Expt.	δ_{PHZ} mm LEM
B1	4.7	4.81	4.05	-	-
F3	-	4.65	6.35	-	1.92
F1	-	7.84	9.95	2 - 3.5	2.20
F0	-	61.19	18.49	-	-

Table 4 ISAT Performance

	ϵ_{tol} = 5E-3	ϵ_{tol} = 8E-3	DI
Total CPU time	16.66 h	9.46 h	31.11 h
Chemistry time	0.0108 s	7.3e-3 s	0.2278 s
Speed up in Chemistry	21	31	-
Speed up in simulation	2	3	-
No. of Records	40500	16500	-

Table 5 15 Step, 19 Species Mechanism

$H + 0.5O_2 = OH$
$H_2 + 0.5O_2 = H + OH$
$HO_2 = 0.5O_2 + OH$
$0.5O_2 + H_2O_2 = OH + HO_2$
$0.5O_2 + 0.5C_2H_2 = H + CO$
$CH_3 + CO + C_2H_4 = 0.5O_2 + CH_4 + 1.5C_2H_2$
$0.5O_2 + 2CH_3 = H_2 + CH_4 + CO$
$0.5O_2 + CH_3 = H + CH_2O$
$0.5O_2 + CH_4 = OH + CH_3$
$0.5O_2 + CO = CO_2$
$0.5O_2 + C_2H_6 = CH_4 + CH_2O$
$H + OH = H_2O$
$H + CH_4 + NO + HCN = 0.5O_2 + 2CH_3 + N_2$
$H + 0.5O_2 + CH_4 + HCN = 2CH_3 + NO$
$0.5O_2 + CH_4 + NH_3 + HCN = H_2O + 2CH_3 + N_2$

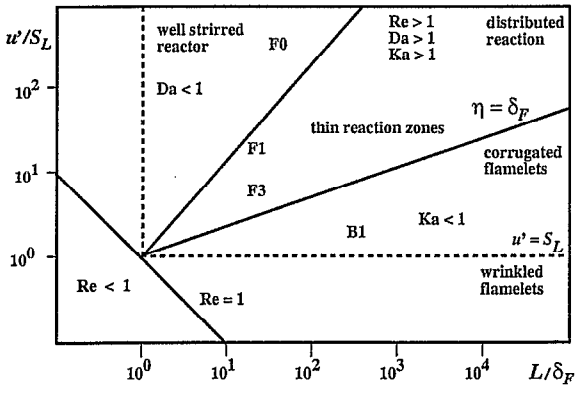

Fig. 1 Diagram of turbulent premixed combustion regimes. The location of the flames simulated in the present study are also shown.

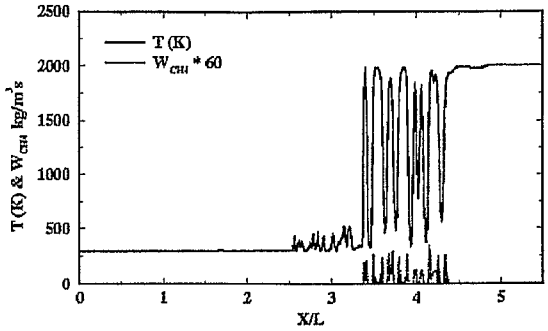

a) Flame B1

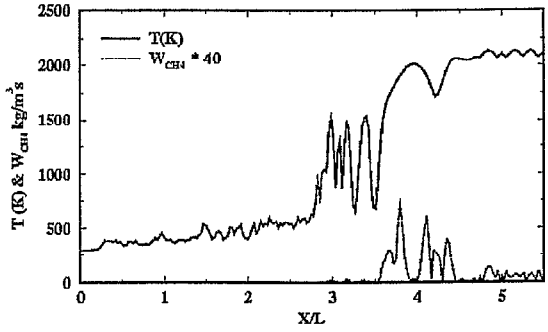

b) Flame F3

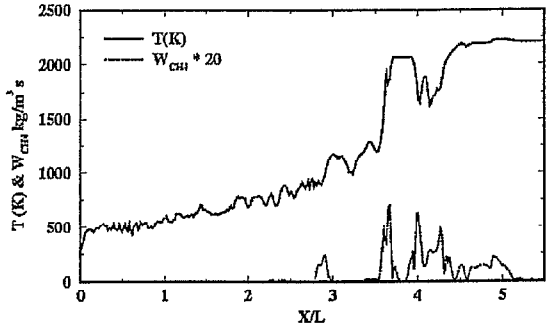

c) Flame F1

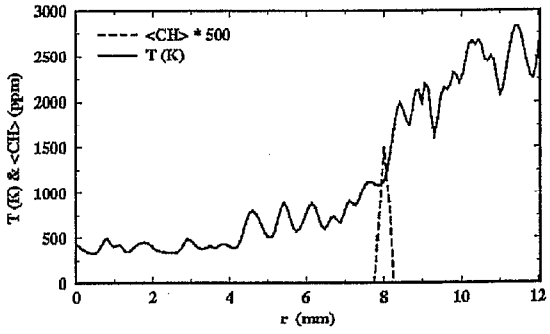

d) Flame F1 from Mansour *et al*[13]

Fig. 2 Instantaneous temperature and $\dot{\omega}_{CH_4}$ for the three flames, B1, F3 and F1 . Scale of $\dot{\omega}_{CH_4}$ is changed for ease of presentation.

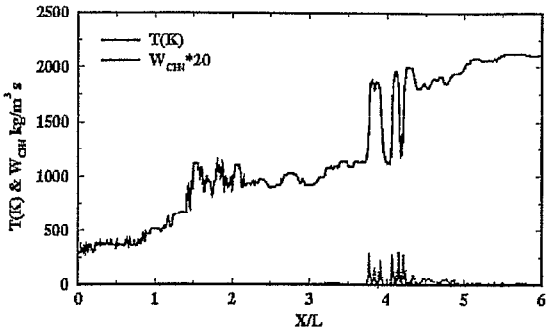

a) Flame F0 resembling flames in thin-reaction-zone

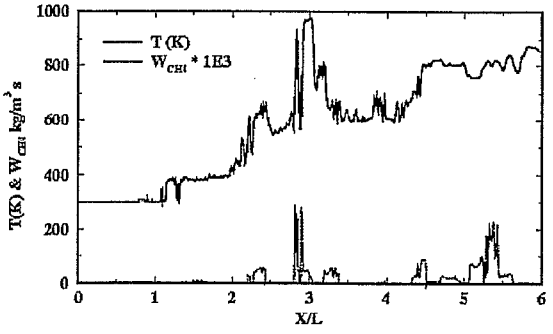

b) Flame F0 when it has been quenched

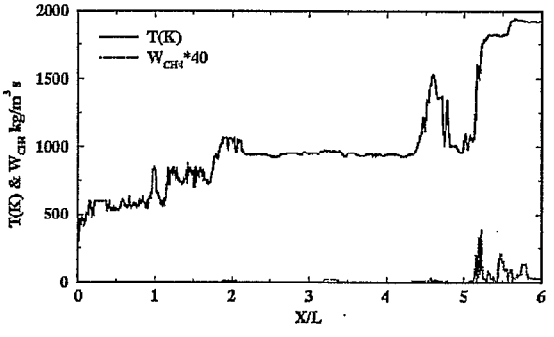

c) Flame F0 showing hot non-reacted holes

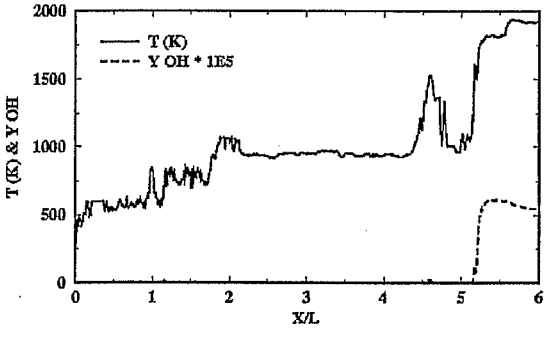

d) Note the absence of OH species in some regions even though temp. is > 1500 K

Fig. 3 Instantaneous temperature and $\dot{\omega}_{CH_4}$ for the flame F0 in well-stirred reactor regime at three arbitrary time instants.

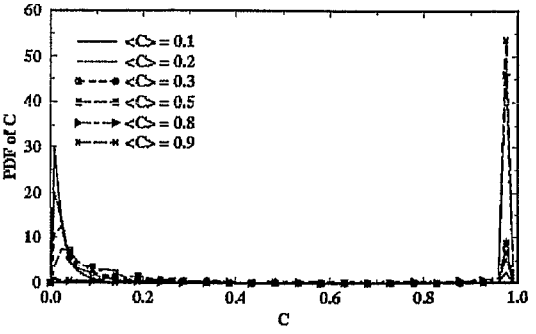

a) Flame B1

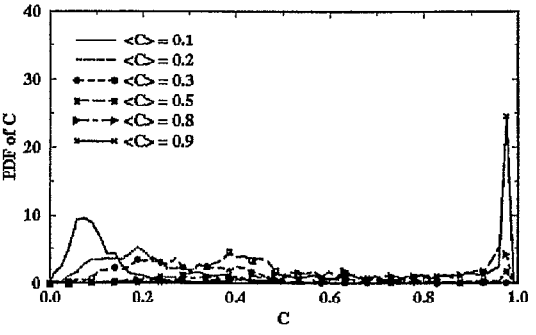

b) Flame F3

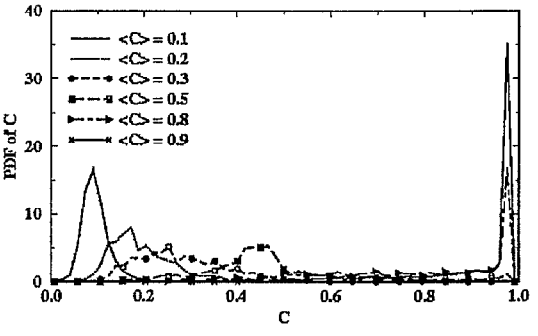

c) Flame F1

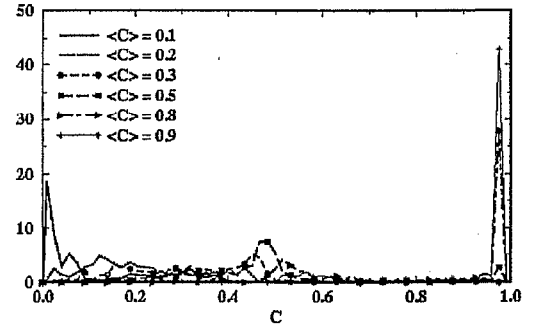

d) Flame F0

Fig. 4 PDF of the progress variable c at six different locations in the four flames. The transition from flamelet structure to the thin-reaction-zones flame structure is apparent in these PDFs.

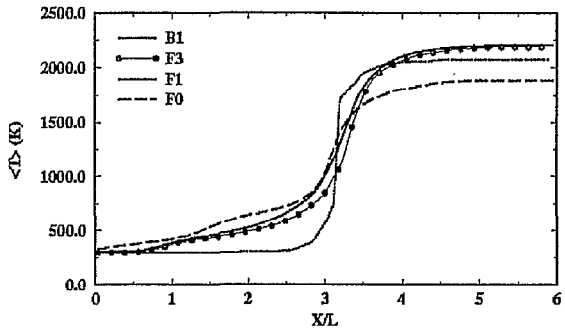

Fig. 5 Mean temperature across the flame brush.

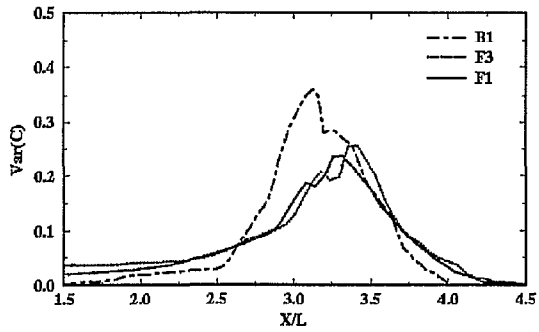

Fig. 6 Scalar variance profiles for all the flames.

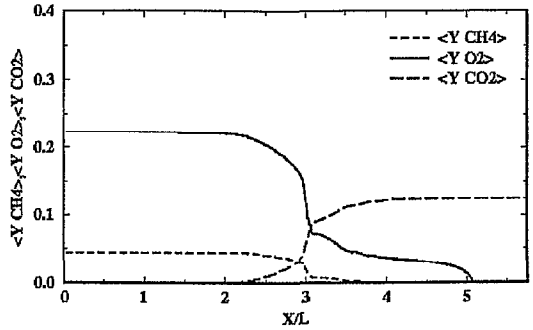

a) Flame B1

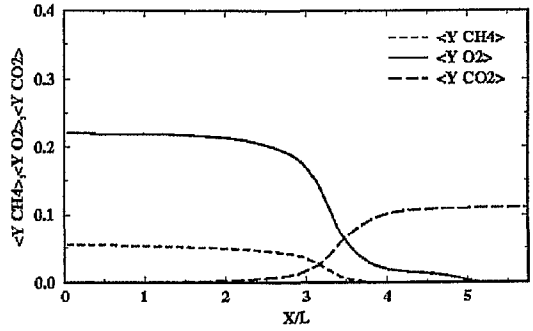

b) Flame F3

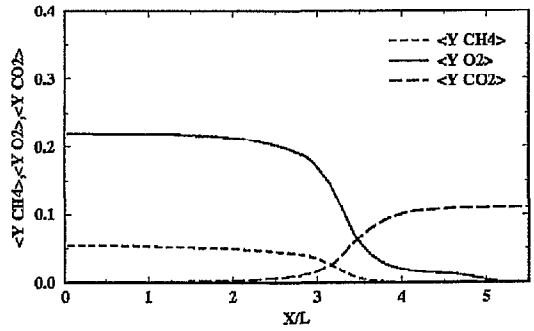

c) Flame F1

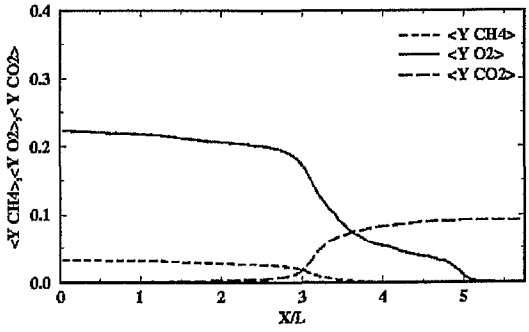

d) Flame F0

Fig. 7 Mean mass fraction profiles of the major species for the flames B1, F3, F1 and F0.

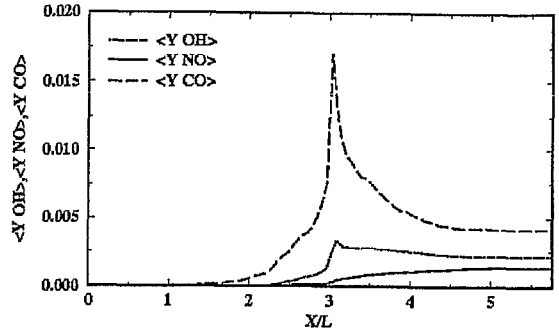

a) Flame B1

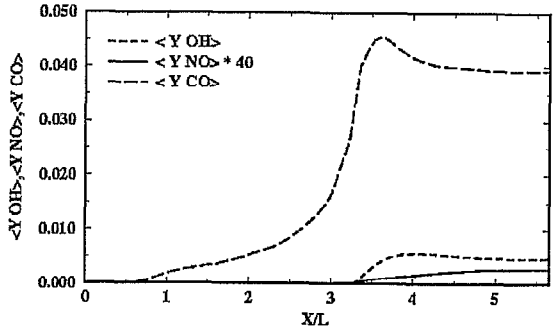

b) Flame F3

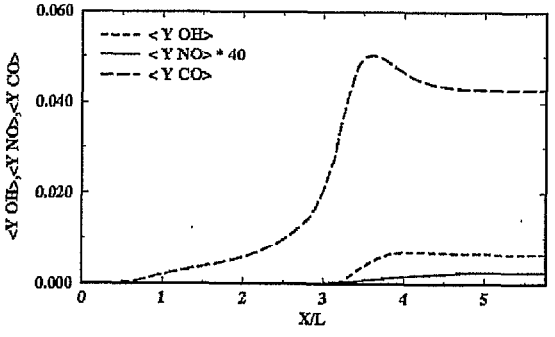

c) Flame F1

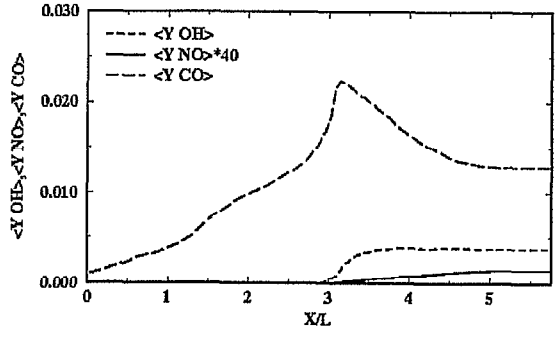

d) Flame F0

Fig. 8 Mean mass fraction profiles of the minor species for the flames B1, F3, F1 and F0.

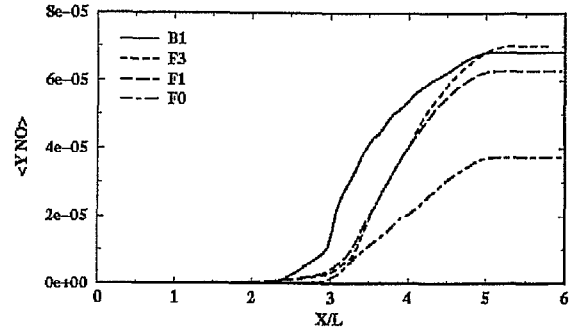

Fig. 9 Mean NOx profiles across the flame brush for the flames B1, F3, F1 and F0.

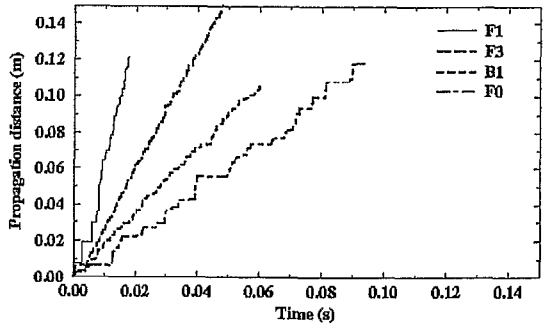

Fig. 10 Time trace of flame front propagation for flames B1, F3, F1 and F0.